Chapter 11

MULTISTAGE AXIAL-FLOW COMPRESSOR AERODYNAMIC DESIGN

The basic concepts introduced in chapter 10 to design an ideal axial-flow compressor stage are easily extended to the design of a complete axial-flow compressor. When the specific working fluid, rotation speed, mass flow rate and inlet thermodynamic conditions are known, the design process can include the influence of total pressure loss and Mach number levels. This is possible as long as the design is restricted to blade operating conditions reasonably close to the design incidence angles, i^*, such that the blades operate in the low-loss incidence angle range where loss coefficients are reasonably constant. This is normal practice at the compressor's design point, i.e., for the mass flow rate and speed condition at which the stages are to be well matched throughout the compressor. An axial-flow compressor design system of this type is unlikely to produce all of the aerodynamic and structural design features desired and all of the off-design operating characteristics required. But it can produce an excellent preliminary configuration to be fine-tuned using the performance analysis of Chapter 9.

The same procedures can be used to design individual stages or blade rows intended for specific applications. For example, it might be used to design replacements for blade rows that are too badly damaged to be reverse-engineered. When this type of design system is available, the benefits of the ideal stage design system of Chapter 10 may seem questionable. Indeed, if sufficient care is taken, this more rigorous design approach may be used in place of the ideal stage design system to generate a standard industrial compressor stage design. It is necessary to avoid imposing restrictions that may preclude using the standard stage for intended applications different from the design conditions used. The procedures defined in this chapter size the compressor annulus to match the specific operating conditions. This imposes a specific stream surface pattern and limits the span of the blades designed to whatever is required to conserve mass. The influence of end-wall boundary layers is also significantly affected by the specific design conditions. If this system is applied at the lowest Mach number level expected and at a higher volume flow rate than is expected to be required, a stage design may be sufficient for general use as a standard stage.

But that typically reduces the design procedure to a more complicated version of the methods described in Chapter 10, effectively nullifying the benefits of the more rigorous models used. Indeed, the design methods of Chapter 10 are often useful for exploring alternative stage performance parameters before attempting a design using the methods of this chapter.

NOMENCLATURE

C = absolute velocity
c = chord
F_g = fractional axial gap between blades
F_{sh} = shroud-to-hub chord ratio
g = axial gap between blade rows
H = total enthalpy
h = blade height
i = incidence angle
i^* = minimum loss incidence angle
m = vortex exponent
n = vortex exponent
P_R = pressure ratio
R = reaction
r = radius
U = blade speed = ωr
W = relative velocity
W_{RE} = equivalent velocity ratio
Z = number of blades
z = axial coordinate
γ = stagger angle
η = efficiency
θ = camber angle
σ = solidity
ϕ = flow coefficient and stream surface slope angle
ψ = work coefficient
ω = rotation speed, radians/sec.

Subscripts

c = parameter on the mean stream surface
h = parameter on hub contour
i = stage number
m = meridional component
s = parameter on shroud contour
θ = tangential component
1 = rotor inlet condition
2 = rotor exit condition
3 = stator exit condition

11.1 THE BASIC COMPRESSOR DESIGN APPROACH

Figure 11-1 illustrates the basic compressor design problem to be solved. The geometry of the end-wall contours and of all blade rows is to be generated, based on specified swirl vortex types and dimensionless performance parameters on the mean stream surface for all stages. As usual, the mean stream surface is defined by the requirement that equal mass flow rates are achieved on both sides of it. To accomplish the design, one of the end-wall contours is defined, while the other is computed from the annulus sizing procedure of Chapter 7. The case illustrated in Fig. 11-1 is typical of an assigned shroud contour design. Since all operating conditions are known, the hub contour can be computed as part of the design solution from simple conservation of mass.

The design procedure to be used is a combination of the stage design method presented in Chapter 10 and a simplified version of the performance analysis of Chapter 9. The performance analysis is simplified by assuming that the loss coefficients are given by the design loss coefficient models of Chapter 6. This is a reasonable approximation as long as the incidence angle is not too different from the design incidence angle. Chapter 6 shows that design loss coefficient is primarily a function of the aerodynamic data. Indeed, from Eqs. (6-35) through (6-37), it is seen that the only geometrical parameter required is the solidity. The flow field throughout the compressor will be generated using specified swirl vortex types and dimensionless stage performance parameters, similar to the approach used in Chapter 10. The simple normal equilibrium equation, Eq. (10-24), is replaced by the meridional through-flow analysis of Chapter 7, using the annulus sizing

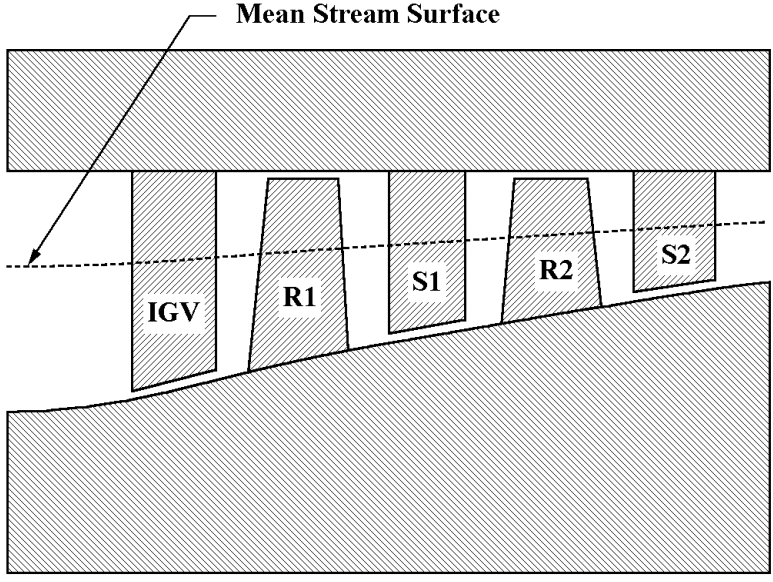

FIGURE 11-1 Compressor Geometry

option. By considering the calculation of solidity as part of the design calculations, the influence of total pressure loss can be included in the flow field calculations. End-wall boundary layer blockage effects are included using the boundary layer analysis of Chapter 8. As long as the design loss coefficient models are valid, this provides a rather accurate and complete prediction of the flow field throughout the compressor. The major approximation required is that streamline curvature effects must be neglected to size the annulus. But once the annulus has been sized, the design process can be repeated using the fixed end-wall geometry mode of the meridional through-flow analysis to allow curvature effects to be included.

The development of this type of compressor aerodynamic design system is much simpler than it may appear. Nearly all of the computational methods required have been presented in previous chapters of this book. The design system used to generate results presented later in this chapter is a good example. It was rather easily formulated directly from the aerodynamic performance analysis. All that was needed was simplification of the blade performance models and revision of the meridional through-flow logic to include the stage performance specifications and airfoil design logic of Chapter 10. Indeed, nearly all of the computer codes needed for this design system already existed in the aerodynamic performance analysis and the ideal stage aerodynamic design system.

11.2 AERODYNAMIC PERFORMANCE SPECIFICATIONS

The aerodynamic performance specifications used are similar to those employed in Chapter 10 for a stage design. For each stage in the compressor, the flow coefficient, work coefficient and reaction on the mean stream surface will be supplied. Parameters on the mean stream surface will be designated by a subscript *c,* and subscripts 1 through 3 will designate successive stations in the stage from rotor inlet to stator exit. Then the performance data for stage number i are given as

$$\phi_{ci} = (C_{mc1} / U_{c1})_i \tag{11-1}$$

$$\psi_{ci} = (H_{c2} - H_{c1}) / U_{c1}^2 = [(r_{c2} C_{\theta c2} / r_{c1} - C_{\theta c1}) / U_{c1} \tag{11-2}$$

$$R_{ci} = 1 - (C_{\theta c1} + C_{\theta c2} r_{c2} / r_{c1}) / (2U_{c1}) \tag{11-3}$$

The definitions of flow coefficient and work coefficient are direct generalizations of the definitions used in Chapter 10. The definition of reaction is chosen for convenience. It will be the true stage reaction only in the case of a repeating stage with a constant-radius mean stream surface. The vortex exponents, n_i and m_i, are also specified for each stage. Then the rotor inlet swirl velocity distribution for any stage is given by

$$C_{\theta 1} = U_{c1}[(1 - R_{ci})(r_{c1} / r_1)^{n_i} - (\psi_{ci} / 2)(r_{c1} / r_1)^{m_i}] \tag{11-4}$$

The swirl velocity distribution at the rotor exit or stator inlet results from the assumption that the work input is constant from hub to shroud. From Eq. (11-2) this requires

$$C_{\theta 2} = [r_1 C_{\theta 1} + \psi_{ci} U_{c1} r_{c1}] / r_2 \tag{11-5}$$

If there is another stage following this one, the stator exit swirl velocity distribution is given by Eq. (11-4), using performance parameters for the next stage, i.e.,

$$C_{\theta 3} = U_{c3}[(1 - R_{c,i+1})(r_{c3} / r_3)^{n_{i+1}} - (\psi_{c,i+1} / 2)(r_{c3} / r_3)^{m_{i+1}}] \tag{11-6}$$

For the last stator, a special specification is required. A convenient choice is to specify the ratio of the exit to inlet swirl velocity as a constant for the last stator, i.e.,

$$C_{\theta 3} / C_{\theta 2} = \text{constant} \tag{11-7}$$

The meridional velocity on the mean stream surface must also be specified as the constant of integration for the normal momentum equation. The specifications used are

$$C_{mc1} = U_{c1} \phi_{ci} \tag{11-8}$$

$$C_{mc3} = U_{c3} \phi_{c,i+1} \tag{11-9}$$

$$C_{mc2} = (C_{mc1} + C_{mc3}) / 2 \tag{11-10}$$

If an inlet guide vane is used, its discharge conditions are identical to the inlet conditions for the first rotor. Similarly, the inlet conditions for an exit guide vane are identical to the discharge conditions for the last stator. At the stations before the inlet guide vane and after the exit guide vane, the swirl velocity is set to zero and it is assumed that the meridional velocity is constant across the adjacent blade row. If additional computing stations are inserted between blade rows, conservation of angular momentum supplies the required swirl velocity distribution from the adjacent station where data has been assigned, and the meridional velocity is set to the same value as that adjacent station. A useful variant on the above equations is to replace U_c and r_c in Eqs. (11-4) through (11-9) by their values at the entrance to the first rotor. This often makes it easier to select appropriate values for the performance parameters by removing the influence of the unknown variation of the mean stream surface radius through the compressor. This is easily included as an option in the computerized design system.

Hence for any assumed annulus and stream sheet geometry, the normal momentum equation, Eq. (7-12), can be integrated if the entropy distributions are known. As discussed in Chapter 7, Section 7.6, the stream surface curvature terms are neglected when sizing the annulus. Thus the compressor design solution is a simple marching process where the solution at each axial computing station is completed before proceeding to the next station. The entropy distributions are computed as part of the solution by computing the design total loss coefficients. As mentioned, this requires knowledge of the blade row solidity, which will be discussed in the next section. Then the annulus area is adjusted as required to balance the known mass flow rate. During this process, the stream sheet pattern is continually changing. Equations (11-4) through (11-10)

are continually applied to update the performance data as the stream sheet geometry changes.

11.3 BLADE DESIGN

The basic process used to design the blades has been described in Chapter 10, Section 10.3. Some minor variations on that process are more appropriate for the present design problem. The following assumptions and specifications have been found to be effective and relatively simple to employ:

- The basic airfoil camberline and profile types from Chapter 4 are specified.
- If required, specify the location of the point of maximum camber, a / c.
- Specify the ratio of the chord at the shroud to its value at the hub and require a linear variation from hub to shroud.
- Specify the thickness-to-chord ratio on the hub and shroud and require a linear variation from hub to shroud.
- Specify the solidity on the mean stream surface.
- Specify the fraction of the axial spacing between computing stations, F_g, that is reserved for the axial gap, g, between blade rows.
- Specify the difference between the actual incidence angle and the design incidence angle, $(i - i^*)$, on the hub and shroud and require a linear variation from hub to shroud.
- Specify the blade tip clearance as a fraction of the shroud radius of the first rotor row.

The blade design procedure is essentially the same as that described in Chapter 10, Section 10.3. The major difference is that the blades must be inserted within a predefined axial distance, since coordinates for one of the end-walls are specified. Here it is necessary to select the number of blades in the blade row and the chords such that the desired axial gap is maintained between blade rows. As illustrated in Figure 11-2, the chord at the hub, which provides the specified axial gap, is

$$c_h = \Delta z_h (1 - F_g) / \cos \gamma_h \tag{11-11}$$

A similar calculation on the shroud contour yields

$$c_s = \Delta z_s (1 - F_g) / \cos \gamma_s \tag{11-12}$$

But these two values are also constrained by the specified shroud to hub ratio, $F_{sh} = c_s / c_h$. This can be used to determine which of the previous two equations specifies a chord necessary to achieve the axial gap. Then the other chord is calculated from F_{sh}. Once the correct chord at the hub is known, the chord at any radius is given by

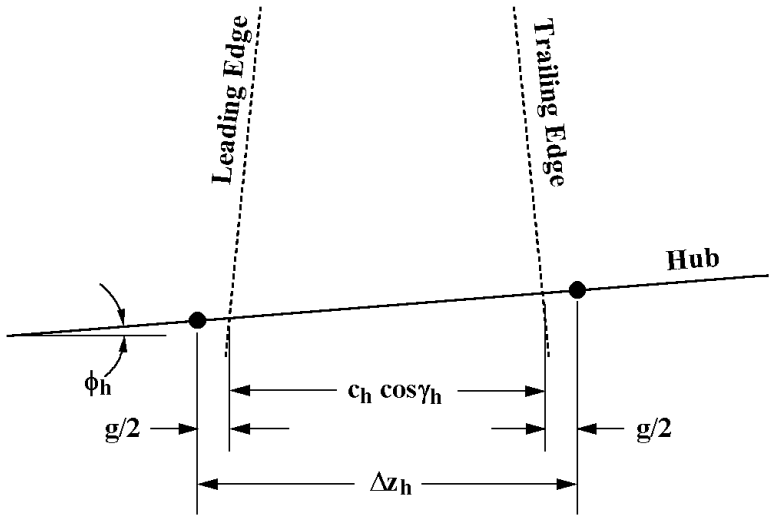

FIGURE 11-2 The Blade Row Axial Gap

$$c = c_h[1 + (r - r_h)(F_{sh} - 1)/(r_s - r_h)] \tag{11-13}$$

If Z is the number of blades in the blade row, the solidity is given by

$$\sigma = [c_h Z/(2\pi r)][1 + (r - r_h)(F_{sh} - 1)/(r_s - r_h)] \tag{11-14}$$

Solving Eq. (11-14) on the mean stream surface, and normalizing it by the result, yields

$$\sigma = \sigma_c \frac{\bar{r}[1 + (r - r_h)(F_{sh} - 1)/(r_s - r_h)]}{r[1 + (\bar{r} - r_h)(F_{sh} - 1)/(r_s - r_h)]} \tag{11-15}$$

Hence the solidity at any radius can be computed from the specified solidity at the mean stream surface before the blades are designed. Since that is the only blade geometrical parameter needed to compute the design loss coefficient, the design flow field analysis can be conducted prior to designing the blades. Then the precise chords and number of blades can be selected using Eqs. (11-11) through (11-14) and the known solidity at the mean stream surface. The largest chords and lowest number of blades permitted by the specified axial gap are selected.

If tip clearance losses are included in the analysis, there is a weak dependence on chord and stagger angle, as can be seen from Eq. (6-86). The end-wall boundary layer analysis also depends on the stagger angle, as seen from Eqs. (8-44) and (8-55). Hence, initial guesses are made for the number of blades and the chord on

the mean stream surface that will yield the desired solidity. The stagger angles on the end-wall contours are approximated from the local flow angles until the first blade design is accomplished. The flow analysis and blade design is repeated until convergence on the chord (or number of blades) is achieved. One repetition is almost always sufficient. At least one repetition is necessary to adequately account for the effect of stagger angle on the end-wall boundary layers.

Another minor difference relative to the procedure of Chapter 10 is that stream surfaces are normally not cylindrical surfaces. The blade geometry used in the flow field analysis needs to be adjusted for streamline slope, using the angle, ϕ, illustrated in Fig. 11-2 for the hub contour. The required corrections have been presented in Eqs. (9-1) through (9-6).

11.4 REFINING THE COMPRESSOR DESIGN

In general, an axial-flow compressor design accomplished by the procedures outlined above will prove a little disappointing when analyzed in the performance analysis of Chapter 9. Even when directly derived from the performance analysis, this design procedure does not normally result in a design that is simply confirmed by it. Since the performance analysis works with assigned end-wall contours, it can directly estimate stream surface slopes and curvatures. In contrast, the design procedure outlined above has only a crude estimate of the sized contour's slope and ignores curvature effects entirely. There are several simple steps that can be incorporated into the design procedure to minimize the differences seen when a performance analysis is conducted on the resulting design.

First, it is very simple to include the capability to repeat the design using the sized contour on the previous attempt as the basis for contour slope calculation. This can be repeated until the contour slopes no longer show a significant change between successive attempts. When that has been achieved, it is very useful to be able to redesign the compressor with the resulting sized contour used directly, instead of sizing the annulus. This will also permit inclusion of stream surface curvature effects, while still generating a flow field consistent with the desired performance parameters and blade geometry consistent with that flow field. It is also useful to constrain the annulus sizing procedure to prohibit an increase in the annulus area in the streamwise direction. When a passage area increase is required, the annulus area can be set to the value at the upstream station and conservation of mass is used to override the local meridional velocity specification.

Resolving inconsistencies with the performance analysis is usually not totally sufficient. When an end-wall contour is computed by the annulus sizing procedures, the resulting contour is likely to be unrealistic, often resulting in erratic variations in coordinates, slopes and curvatures. Refining the dimensionless performance parameters can reduce this erratic behavior. But that is a rather tedious process, and involves changes in the performance parameters that are really physically insignificant. It is much more effective to include procedures to permit smoothing and editing the contour coordinates. Then the design process can again be repeated with the revised contour to produce the desired performance. A simple smoothing procedure that has been found effective is illustrated in Fig. 11-3. In this case, the shroud has been sized with somewhat erratic results.

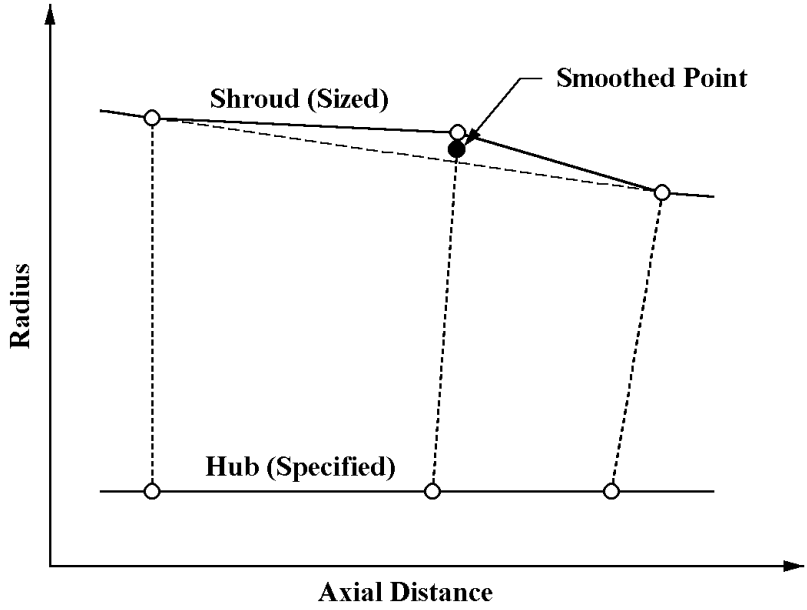

FIGURE 11-3 Contour Smoothing

The approach used is performance of a simple linear interpolation between adjacent axial computing stations to determine an alternate radius on the quasi-normal of interest. Then a smoothed point is defined as an average of the actual and interpolated points. The smoothed points can be used directly for all interior quasi-normals. Alternatively, smoothing can be omitted at certain quasi-normals, typically either at the rotor inlet or rotor discharge quasi-normals. That may be desirable to preserve key elements of the sizing process. It is best to implement this contour smoothing as an interactive process where the smoothed contour is displayed graphically, with the original contour points in the background. Then the designer can try alternate smoothing strategies to select the most promising method. This can also include provision to directly edit some coordinates that do not adequately respond to the smoothing procedures alone. That is fairly common for quasi-normals upstream of the first rotor and downstream of the last stator. The same contour smoothing procedures can be very useful in the performance analysis, particularly when the annulus sizing procedure is used. Indeed, these smoothing procedures were used for the two standard repeating stage compressor designs described in Section 10.11

If properly implemented, all of these procedures for refining the design can be employed with very little effort on the part of the designer. If they are not accomplished here, they will almost certainly need to be accomplished manually in the performance analysis. That will involve much more effort, particularly since the blade designs will require modification during the process and the

desired performance parameters will almost certainly be compromised. By incorporating them in the compressor aerodynamic design system, performance goals and blade design are handled automatically. This results in a dramatic reduction in fine-tuning the design using the performance analysis.

11.5 AN AXIAL-FLOW COMPRESSOR DESIGN EXAMPLE

The application of this axial-flow compressor aerodynamic design procedure will be illustrated by developing various alternate designs for the second ten-stage compressor designed in Chapter 10 using a standard repeating stage. The procedures in this chapter will be employed to design the end-wall contours and the geometry of the 22 blade rows required. NACA 63-series inlet guide vanes will be used while NACA 65-series blades will be used for all other blade rows. All designs will limit the rotor tip relative Mach numbers to a maximum value of 0.8. All compressor designs will be sized to specified performance parameters with a constant hub-contour radius. The shroud contours will be smoothed and refined as described in the previous section of this chapter.

The first example is designated as Compressor A. It is based on stage performance parameters similar to those achieved in Chapter 10 with the standard repeating stage. Figure 11-4 shows the stage mean stream surface performance parameters specified. A simple linear variation with stage number was used,

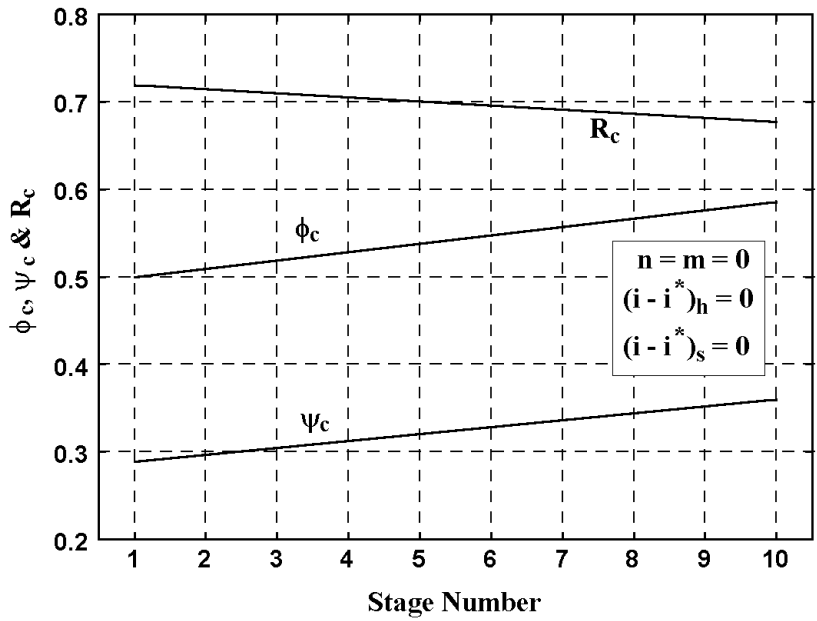

FIGURE 11-4 Stage Design Data for Compressor A

where data for the first and last stages were obtained from the standard-stage compressor performance analysis shown in Fig. 10-38. Then the work coefficient for the last stage was adjusted by trial and error to produce approximately constant-camber, untwisted stator blades throughout the compressor. After sizing the annulus, the shroud contour was smoothed twice, each time holding the rotor inlet shroud radii constant. Figure 11-5 shows the end-wall contours obtained from that process. Then the flow field was predicted for these end-wall contours using the approximate normal equilibrium model described in Section 7.6 for the meridional through-flow analysis to obtain the final blade row designs. All blades were designed to operate at their design incidence angles, while matching with the predicted flow field. The computerized design system used makes this a rather simple process. Once the initial design specifications had been entered, the entire design process for Compressor A was completed in about five minutes.

Then Compressor A was analyzed using the performance prediction methods of Chapter 9. Consistent with the aerodynamic design approach, the approximate normal equilibrium model described in Section 7.6 was used for the performance analysis. The predicted difference between the incidence angles and the design incidence angles on the hub-and-shroud contours is shown in Fig. 11-6. The performance analysis supplies incidence angles rounded off to the nearest 0.1°. Hence, it can be seen that the deviation from the intended incidence angle match was less than 0.15° in all cases. Comparison of the calculated incidence angle

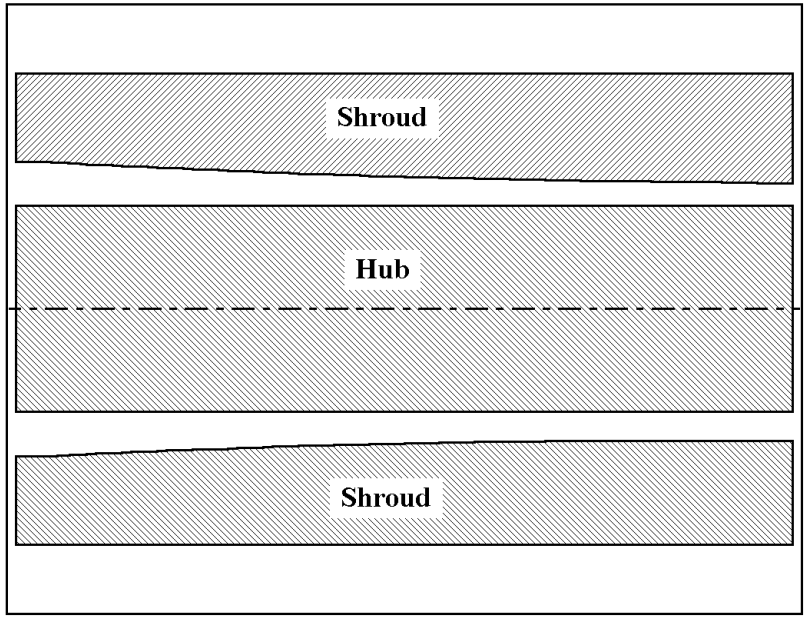

FIGURE 11-5 End-Wall Contours of Compressor A

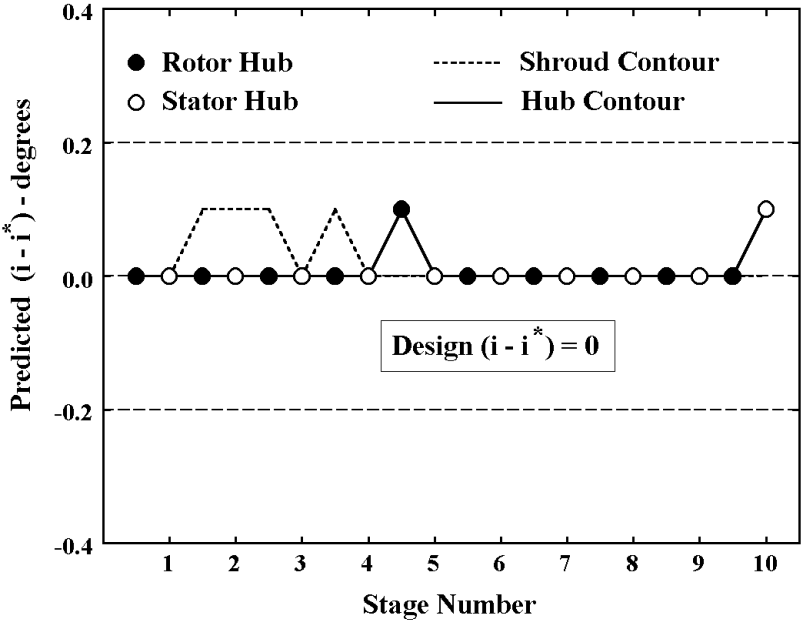

FIGURE 11-6 Predicted Incidence Angle Match

match with the design specifications is the best way to validate the aerodynamic design system. Even minor differences between the design system and the performance analysis will produce significant differences in the incidence angles that cascade to rather large values in the rear stages of a multistage compressor. The results in Fig. 11-6 are fairly typical of what can be achieved by a properly formulated aerodynamic design system.

Figure 11-7 shows a predicted performance map for Compressor A, along with results from Fig. 10-38 for the standard-stage design; The two designs are quite similar. The present design achieves a larger pressure ratio and improved surge margin at design speed, but at the expense of a reduced maximum flow capacity. Careful review of the standard stage compressor performance analysis showed that the stages exhibit slightly positive values of $(i - i^*)$ in the front stages, whereas the nearly ideal matching shown in Fig. 11-6 was achieved for Compressor A. Hence the differences in performance are not unexpected nor are they particularly significant. A minor re-matching of the stages in either of these designs could easily result in performance nearly identical to that of the other design. Clearly, the substantial cost advantage offered by the standard repeating stage compressor with its constant camber, untwisted stator blade is achieved with little compromise. The nearly ideal stage matching with completely arbitrary blade geometry used in the design of Compressor A does not result in any significant performance improvement. In this specific example, the most significant benefit

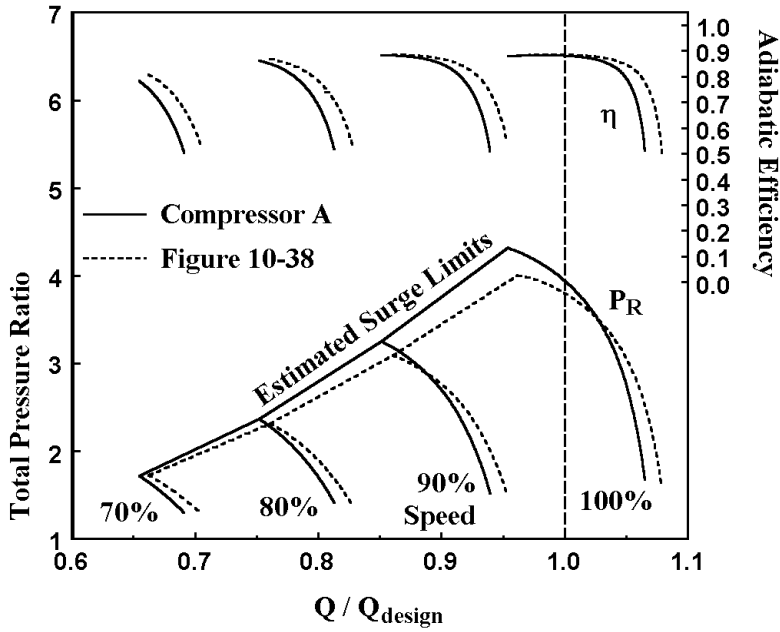

FIGURE 11-7 Performance of Compressor A

obtained from the present aerodynamic design system is that the design of Compressor A was much easier to accomplish than the design of the standard repeating-stage compressor.

It should not be concluded that this more general aerodynamic design procedure does not offer the potential for improved performance over a standard stage compressor design. Since the design of Compressor A is based on specifications obtained from a performance analysis of a repeating stage compressor, some similarity to a repeating stage compressor is to be expected. Figure 11-8 shows the basic blade geometry on the hub contour, where the radius is constant. It can be seen that the design does approximate a repeating stage configuration. The geometry for the last stator has been omitted, since it is rather arbitrary, depending directly on the specification of how removal of the swirl from the last rotor is to be split between the last stator and the exit guide vane. Although not obvious from Fig. 11-8, it is simply stated that a standard constant-camber, untwisted blade could easily be substituted for the stator blades designed for Compressor A, but with stagger angles varying through the machine. However, the rotor blade geometry varies too much through the machine to permit substitution of a standard rotor blade. Hence the design of Compressor A was really constrained to approximate the repeating-stage design of Chapter 10. Although the blade geometry was not constrained, this added flexibility was not used to much advantage.

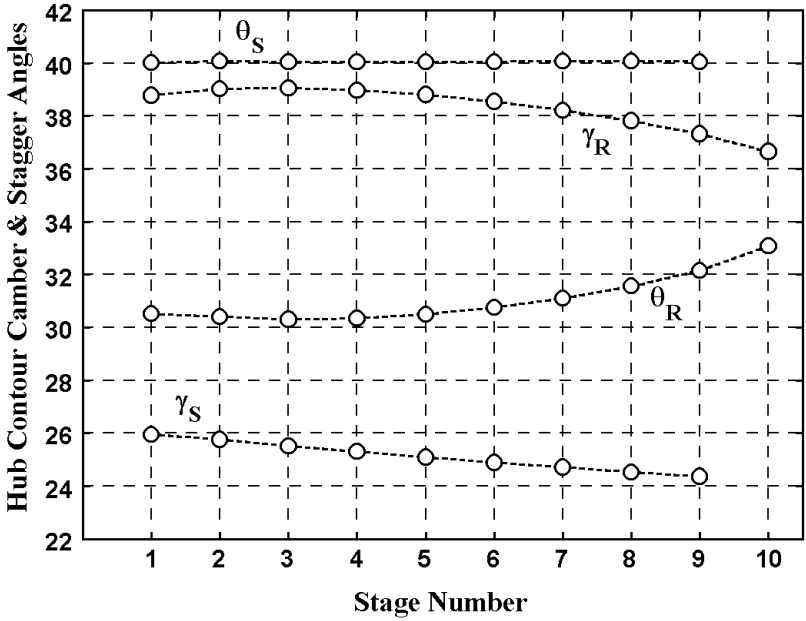

FIGURE 11-8 Hub Contour Blade Geometry

11.6 THE DISTRIBUTION OF STAGE PERFORMANCE PARAMETERS

More effective use of the general aerodynamic design procedure is possible by simply applying a distribution of stage performance parameters through the compressor. The variation in stage performance parameters shown in Fig. 11-4 for Compressor A is somewhat misleading, since it really only corrects the stage performance parameters for the variation in mean stream surface radius. A compressor design establishes the annulus area distribution and blade geometry suitable for the design rotation speed. When the compressor is operated at speeds less than the design speed, the work per stage is reduced, such that the increase in gas density is no longer sufficient for the stages to remain matched. The rear stages will operate at flow coefficients higher than their design values, with a corresponding reduction in work per stage. The front stages will have the highest work per stage and will be the first stages to stall. The rear stages contribute much less work and will limit the compressor's flow capacity. When the compressor is operated at speeds greater than design speed, the opposite trend will occur. The front stages produce more work and a larger increase in gas density than intended. Downstream stages tend to operate at flow coefficients less than their design values, with a corresponding increase in work coefficient. Generally, the rear stages have the highest work per stage and will be the first stages to stall. The front stages will contribute less work input and will limit the compressor's flow

capacity. In effect, the annulus area distribution is too small for operation at low speeds and too large for operation at high speeds.

It follows that the stages least affected by variations in rotation speed are the mid-stages. In a properly designed compressor, the mid-stages will normally operate closer to their design operating conditions than either the front or rear stages, and are less likely to be responsible for the compressor's stability or flow capacity limits. Hence it is reasonable to employ more highly loaded mid-stages, with more conservative loading of the front and rear stages. Stage loading is not a well-defined term. Some investigators use it to refer to the stage work coefficient; others use it to refer to the flow diffusion across the blade rows. In the present context, both aspects must be considered. Higher work coefficients will be used for the mid-stages. Somewhat greater flow diffusion may be attempted, since the mid-stages are expected to operate over a narrower flow coefficient range than either the front or rear stages. However, excessive flow diffusion must still be avoided. The evaluation of flow diffusion used here will be the relative velocity ratio across the blade rows, W_2 / W_1, or the effective velocity ratio, W_{RE}, defined in Eq. (9-16). The two parameters are approximately the same, but the latter has been used as the basis of the blade stall criterion developed in Chapter 9. In Chapter 10, it was shown that the work coefficient can be increased without increased flow diffusion if the flow coefficient is also increased. That will require a departure from using Smith's (1958) recommended flow coefficient of 0.5 based on the recovery ratio of Eq. (10-36). From Figs. 10-7 through 10-9, it is apparent that large positive values of the recovery ratio are achieved for a fairly wide range of flow coefficients. Also, the risk of lower recovery ratios should be much less at the mid-stages, since they are expected to experience less severe operating conditions than the front and rear stages.

The present aerodynamic design system makes it relatively simple to develop a suitable distribution of stage performance parameters. To illustrate the process, Compressor B was designed for the same design mass flow, rotation speed and hub contour as that used for Compressor A. The stage performance parameters used are shown in Fig. 11-9. The design system used for this example permits specification of stage performance data at an arbitrary number of stages, with linear interpolation for the other stages. In this case, specifications were provided for stages 1, 2, 3, 4, 8 and 10. The distribution of ϕ_c starts with a value of 0.55 for the first stage and ramps up through the front stages to permit an increase in ψ_c without unacceptable diffusion levels. Initial distributions of K_c and R_c were assumed. K_c was assigned instead of ψ_c to provide more direct control over the diffusion levels in the stages. The distributions of K_c and R_c were adjusted by trial and error until acceptable diffusion levels were achieved through the compressor. K_c was adjusted to achieve acceptable levels of $W_{RE,}$ and R_c was adjusted to approximately balance the diffusion load between the rotor and stator for all stages. Fig. 11-9 shows the key values of W_{RE} obtained on the hub-and-shroud contours for the design mass flow and rotation speed. Stator shroud values are omitted from figure 11-9 since they pose no problem for the constant swirl vortex type. Similarly, the last stator is omitted since its diffusion load can be controlled independent of the stage performance data. Hence the mid-stages feature higher work and more diffusion than either the front or the rear stages. Based on the previous discussion, it might be expected that the ϕ_c

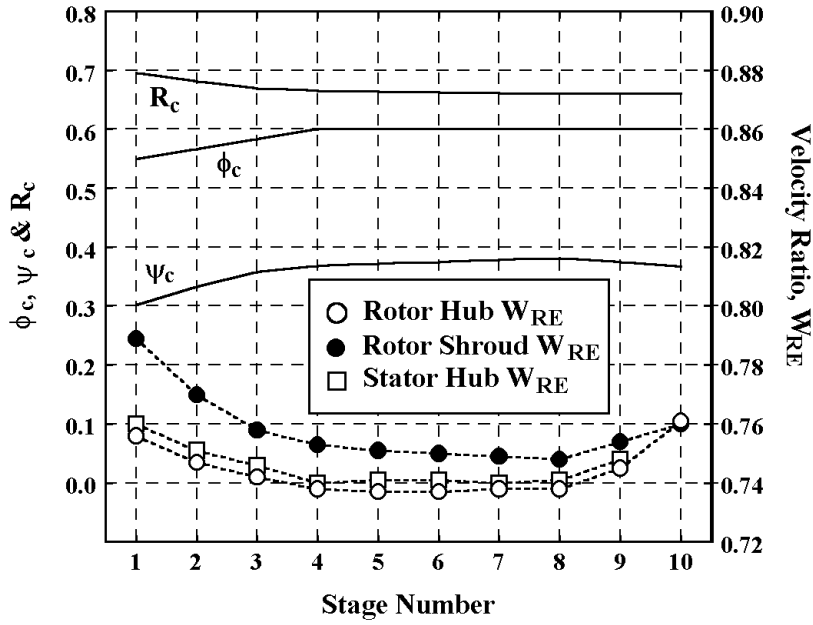

FIGURE 11-9 Stage Design Data for Compressor B

distribution should ramp down to lower values in the rear stages. That is generally not advisable due to adverse effects on the end-wall boundary layers. The end-wall boundary layers are relatively thick in the rear stages, such that a reduction in meridional velocity can easily lead to excessive boundary layer blockage. Indeed, the interaction between the end-wall boundary layer analysis and the annulus sizing calculations can become so severe that convergence is virtually impossible. That is the main reason why the present design system constrains the annulus sizing to preclude an increase in passage area in the streamwise direction. Had ϕ_c been ramped down through the rear stages, that constraint probably would have caused the lower values to be ignored anyway. To further illustrate the flexibility available for tailoring the stage performance distributions, Compressor C was designed using the design data shown in Fig. 11-10. This design followed the same strategy as that used for Compressor B, but uses higher stage flow coefficients to permit higher work coefficients. Figure 11-10 also shows the key values of W_{RE} obtained. Note that compressor C achieves higher work per stage than Compressor B, but has similar flow diffusion characteristics.

Figure 11-11 compares performance predictions for Compressors A, B and C. Polytropic efficiency is shown for this comparison to avoid the thermodynamic effect due to pressure ratio discussed in Chapter 2. Both the pressure ratio and the stable operating flow range for Compressor B are generally improved relative to Compressor A. There is a slight loss in stable operating range at the design speed, but improved stability at other speeds. There is a slight reduction in efficiency due

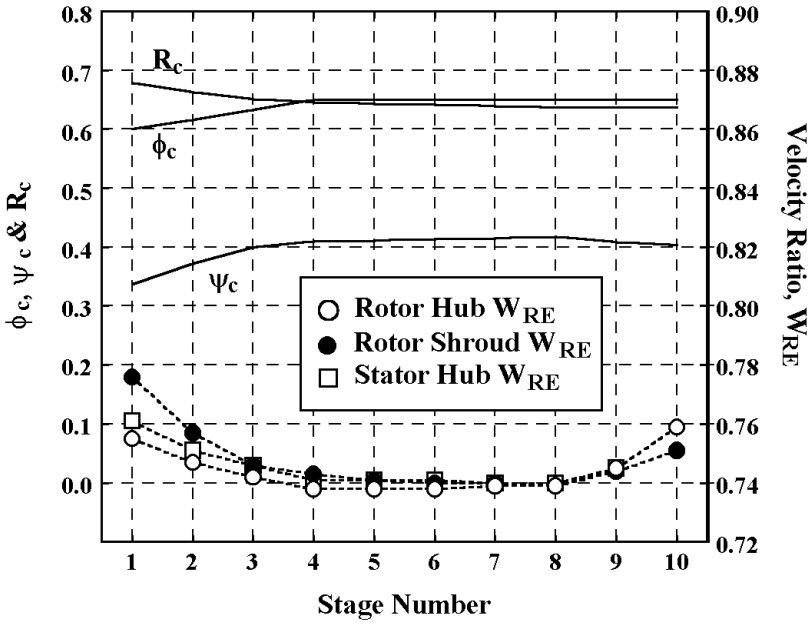

FIGURE 11-10 Stage Design Data for Compressor C

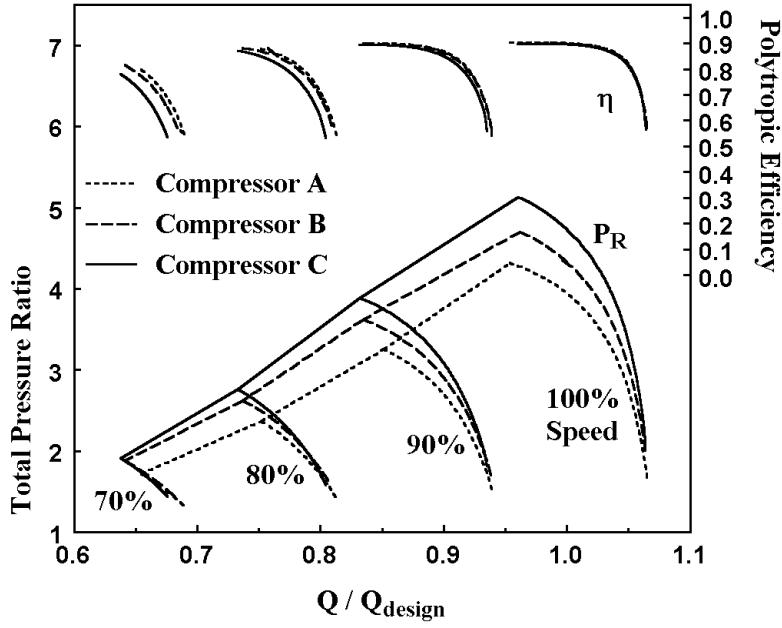

FIGURE 11-11 Predicted Performance Maps

to the reduced aspect ratios that result from the higher values of ϕ_c and pressure ratio. This requires use of lower values of blade height, h, in the rear stages, resulting in higher predicted loss coefficients as seen from Eq. (6-99). The estimated surge limit for all three compressors is based on stall criterion #3 of Chapter 9. At design speed, this initially occurs in the mid-stages, whereas at other speeds the front stages stall first. The improved stable operating range is particularly noticeable at the lowest speed. As expected, the reduced diffusion in the front stages has permitted the compressor to operate more effectively at low speeds. Note that the improved stable operating range is also present in Compressor C, even though its design pressure ratio is higher than that of Compressor B. Clearly, careful control of the blade row diffusion characteristics is a primary consideration with regard to improved compressor performance. But there are certainly other considerations that may not be reflected by current aerodynamic performance prediction technology. All designers certainly have strong incentive to favor large values of ϕ_c and ψ_c to increase the mass flow per unit frontal area and to reduce the number of stages required. Whether the goal is reduced size and weight or reduced cost, the incentive is always present. Nevertheless, recent design trends appear to favor lower values of ϕ_c and ψ_c based primarily on perceived benefits to performance. Possible explanations were discussed in Section 10.4 of the previous chapter. Other investigators appear to believe that the explanation lies in the end-wall boundary layer behavior.

While lower values of ϕ_c and ψ_c may be preferred, the designer has considerable flexibility in regard to stage performance parameters. Rather large values of ϕ_c and ψ_c have been used with success. For example, Fig. 11-12 shows calculated stage performance parameters obtained from the performance analysis of the NACA 10-stage subsonic compressor of Fig. 9-4. This compressor achieved respectable performance, considering the state-of-the-art in axial-flow compressor aerodynamic technology fifty years ago when it was designed. Yet rather large values of ϕ_c and ψ_c were used in most of the stages. For illustration, Compressor D was designed using the highest values of ϕ_c and ψ_c allowed by the rotor tip relative Mach number limit imposed on the previous designs. The same operating conditions and design strategy as those for Compressors B and C were used. Figure 11-13 shows the design parameters used and the flow diffusion characteristics obtained. It was not possible to balance the flow diffusion as well for this case. Blade stall in a constant swirl vortex stage almost always occurs first on the hub contour, usually in the stators. Hence, lower rotor shroud velocity ratios were accepted so that the hub contour flow diffusion characteristics could be maintained in a manner similar to that of Compressors B and C. Indeed, for any compressor, the blade sections at the hub must operate over a much wider incidence angle range than the rotor shroud blade sections. Figure 11-14 compares the predicted performance maps for Compressors B, C and D. Again, polytropic efficiency is shown for this comparison to avoid the thermodynamic effect due to pressure ratio discussed in Chapter 2. It is seen that aspect ratio effects have an adverse effect on efficiency, particularly for Compressor D. A special performance analysis of Compressor D using a larger number of shorter chord length blades in the rear stages produced essentially the same efficiency at design speed as for the other two designs. This indicates that the reduction in design speed efficiency seen in Fig. 11-14 is due to aspect ratio effects rather than being a direct result of

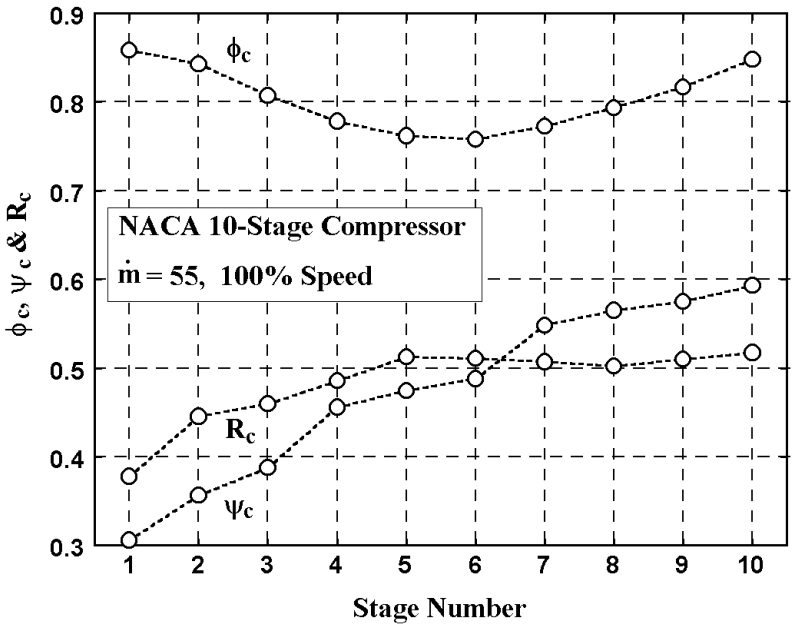

FIGURE 11-12 Actual Stage Performance Data

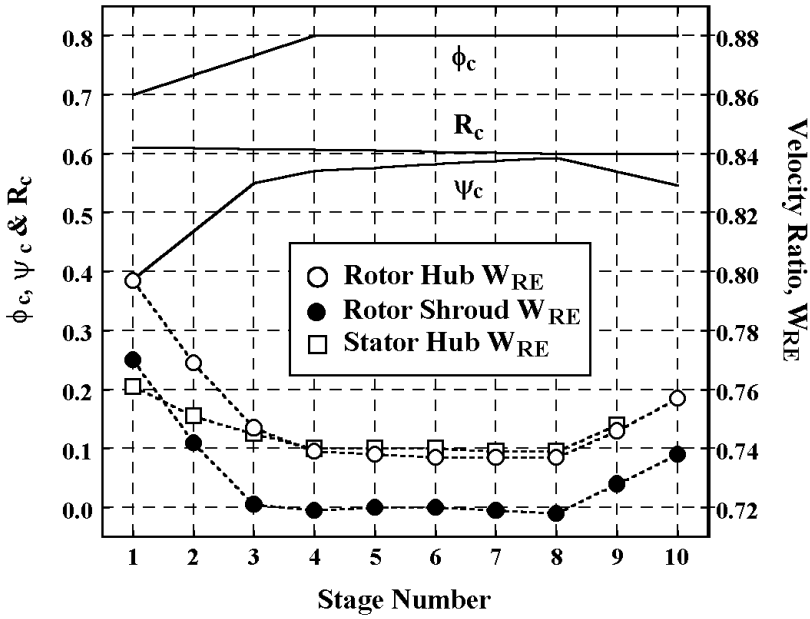

FIGURE 11-13 Stage Design Data for Compressor D

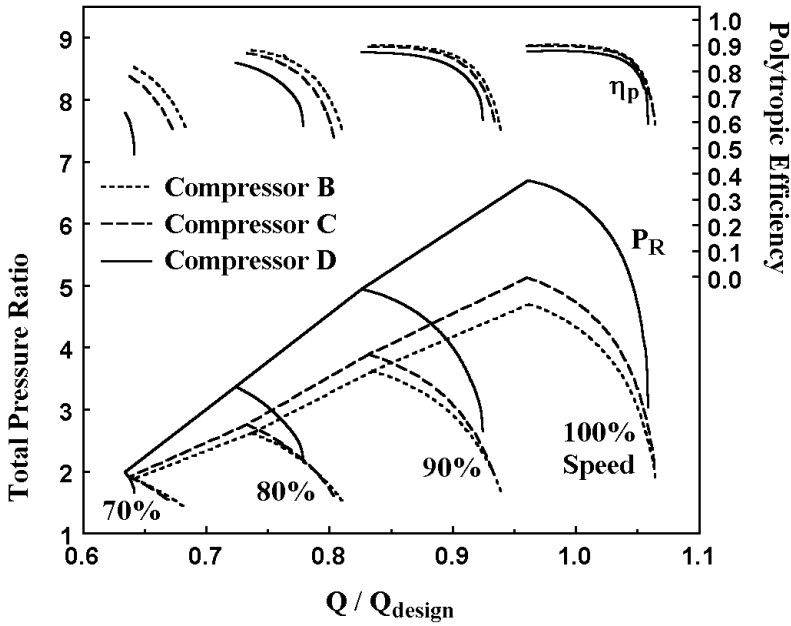

FIGURE 11-14 Effect of ϕ_c on Performance

the values of ϕ_c and ψ_c used in the design process. At lower speeds, both efficiency and stability appear to deteriorate as higher values of ϕ_c and ψ_c are used in the design process. Hence the performance analysis of chapter 9 indicates some adverse effects at off-design speeds from designing with higher values of ϕ_c and ψ_c. But it really does not indicate any significant influence of ϕ_c and ψ_c on the performance at design speed. It is now generally accepted that designing with lower values of ϕ_c and ψ_c offers definite performance benefits. It is clear that those benefits are not completely quantified by the performance analysis of Chapter 9.

The present design system makes it rather simple to tailor the distributions of stage performance parameters and blade row diffusion characteristics to emphasize aerodynamic features considered important to the design objectives. This is more clearly illustrated by another simple example: Suppose that Compressor B must operate on a load line that lies too close to the surge line at the lower rotation speeds. Compressor E is to be designed with the objective of improving the low-speed surge margin while maintaining the same basic design speed performance as Compressor B. The annulus contour and the number of stages are to be identical to Compressor B. In effect, the design of Compressor E is constrained to be identical to Compressor B except for the blade geometry. Figure 11-15 shows the stage design parameters and flow diffusion characteristics used to achieve this objective. Figure 11-16 illustrates a load line that might require this redesign and compares the predicted performance maps for the two compressors. Comparison with Fig. 11-9 shows that the design of Compressor E differs from that of

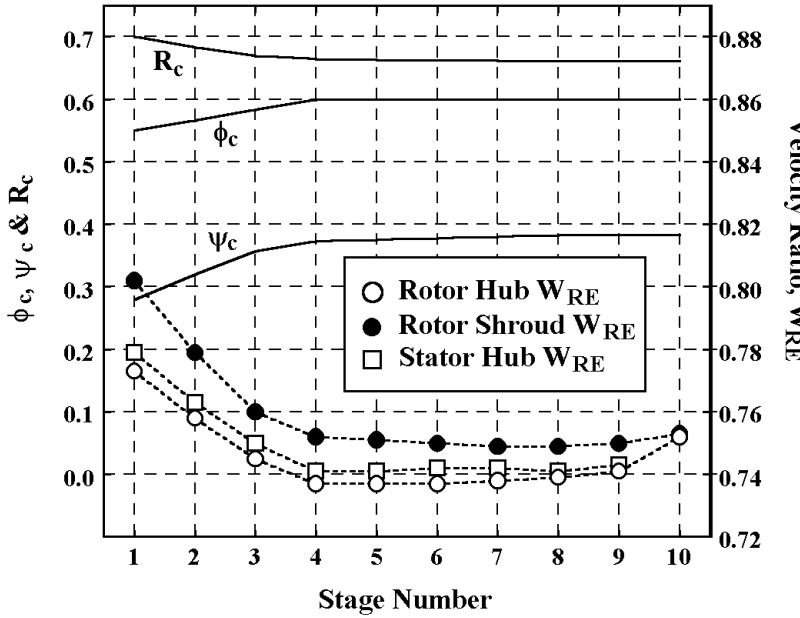

FIGURE 11-15 Design Data for Compressor E

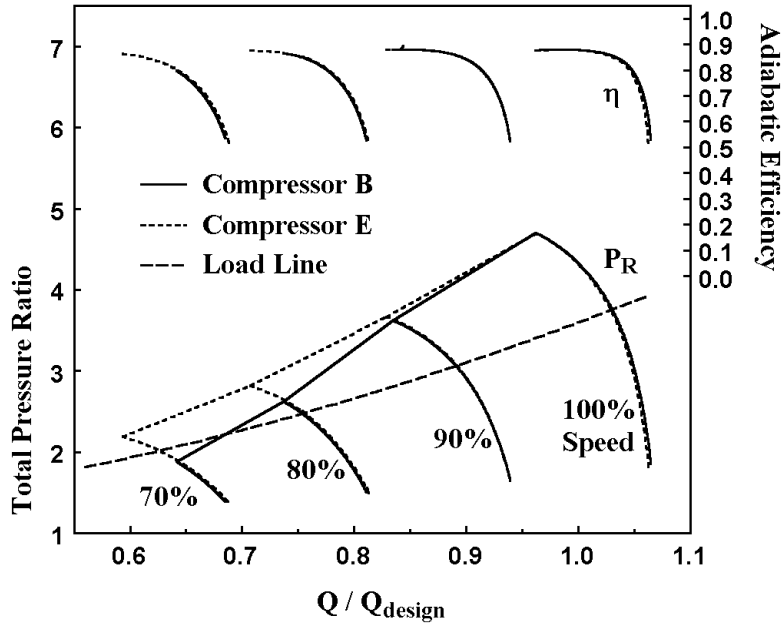

FIGURE 11-16 Performance of Compressors B and E

Compressor B by a fairly modest shifting of the stage loading from the front to the rear. It can be seen that a substantial improvement in the low-speed surge margin has been achieved with minimal effect on the design speed performance.

11.7 THE SWIRL VORTEX TYPE

Chapter 10 reviews the influence of swirl vortex in the context of a single, repeating stage design. The present aerodynamic design system can be used to evaluate alternate vortex design types in the context of multistage compressors designed with the tailored distributions of stage performance parameters and flow diffusion characteristics. Compressor B is used as the constant swirl vortex design for this comparison. Alternate compressor designs have been generated using the free vortex and constant reaction vortex types. Although the constant reaction vortex type was not very effective for the single stage designs in Chapter 10, the present application is better suited to this type of vortex. The major weakness seen in Chapter 10 is the highly distorted meridional velocity profiles. The higher hub-to-shroud radius ratio used in the present case will reduce the influence of that profile distortion. Figures 11-17 and 11-18 summarize the design data used for the alternate designs. The alternate designs are based on the same operating conditions and distribution of ϕ_c as Compressor B. The distributions of R_c and ψ_c are adjusted to produce flow diffusion characteristics similar to those in Fig. 11-9. The free vortex and constant swirl vortex types have very similar flow diffusion

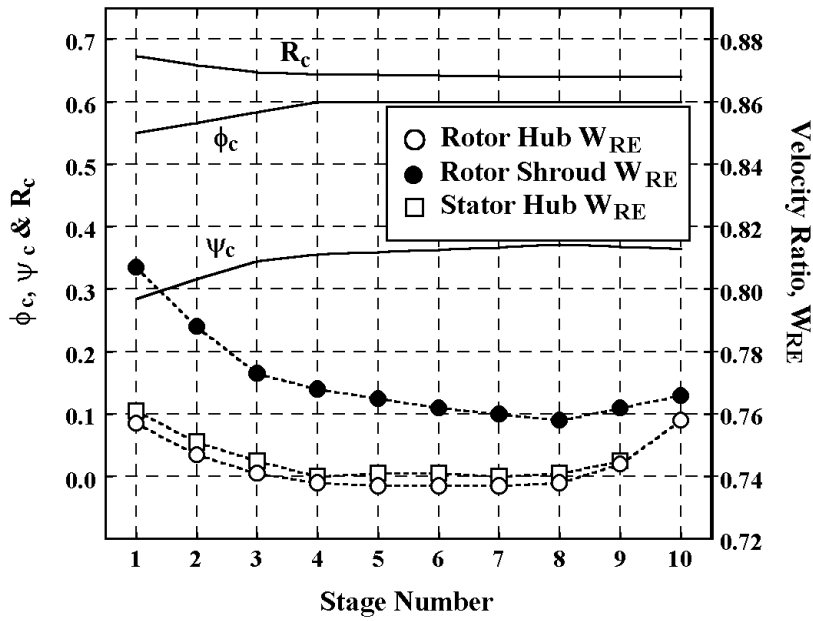

FIGURE 11-17 Free Vortex Design Data

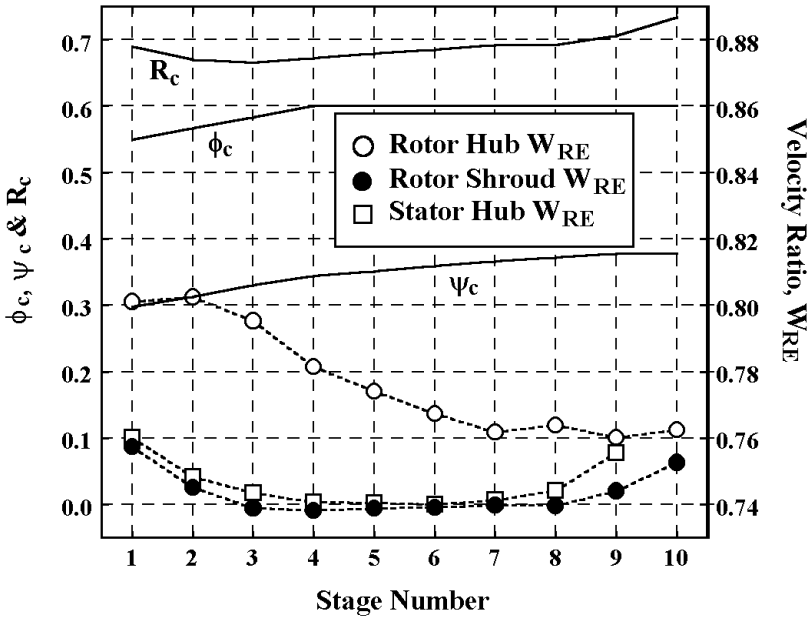

FIGURE 11-18 Constant Reaction Vortex Design Data

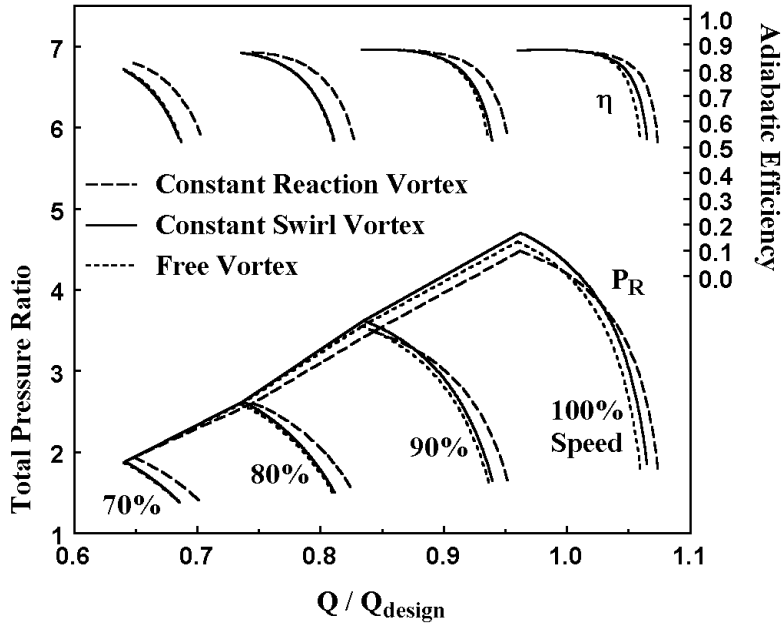

FIGURE 11-19 Effect of Vortex Type on Performance

characteristics. Only minor modifications to the data in Fig. 11-9 were needed to obtain the results shown in Fig. 11-17. The flow diffusion characteristics of the constant reaction vortex type are quite different. There the rotor velocity ratios on the shroud had to be balanced against the stator hub values for most of the stages. The stator hub flow diffusion was expected limit stability, which was subsequently confirmed by the performance analysis. Hence emphasis was placed on achieving similar stator hub velocity ratios as those used for the other two vortex types, without excessive diffusion at other locations. Fig. 11-19 compares the predicted performance maps for the three compressor designs. Note that the flow range from the design point to surge at the design speed is essentially identical for all three compressors. The performance predictions indicate that the stator hub flow diffusion characteristics have much more influence on stability than the swirl vortex type. It is also seen that the compressor efficiency level is rather insensitive to the swirl vortex type used. The constant reaction vortex design low speed characteristics are shifted in flow relative to the other two designs, but the efficiency levels are comparable for all designs. The free vortex design produced a slightly lower pressure ratio than the constant swirl vortex design, but otherwise yields performance very similar to Compressor B. The constant reaction vortex type yields a significantly lower pressure ratio than Compressor B. Possibly this could be improved somewhat with further refinement, but it seems clear that the constant reaction vortex design does not offer any advantage over the other two designs. The constant reaction vortex type is much harder to work with and has definite limitations with regard to acceptable hub-to-shroud radius ratios. Hence there seems to be little reason to consider using it for axial-flow compressor design.

The blade geometry resulting from the various swirl vortex types is also a significant consideration. Figures 11-20 and 11-21 compare camber and stagger angles for the rotor and stator blades for the first stage of the three compressor designs. The first stage is selected since it has the longest blades, but comparisons of blades in other stages would be quite similar. The rotor blades for the three designs are so similar that there is no clear preference. The stator blade geometry is very dependent on the swirl vortex type. The constant swirl vortex produces a stator that can be well approximated by a constant-camber, untwisted blade. This will be the easiest to manufacture and costs the least. The free vortex stator can be well approximated by a constant-camber blade with a linear twist. This would be the second choice with regard to cost and ease of manufacturing. The constant reaction vortex requires a more complicate camber angle distribution, but a linear twist might be used to approximate the stagger angle distribution. The characteristic increase in camber angle near the shroud is apparent. This would be much more pronounced if a lower hub-to-shroud radius ratio were used, as can be seen in Fig. 10-32. Thus, the complexity of the stator geometry is another reason to avoid the constant reaction vortex type.

The present aerodynamic design system makes it relatively simple to investigate the influence of alternate swirl vortex types. Here, three quite different vortex types have been compared for a sample problem quite typical of an industrial axial-flow compressor. Based on this comparison, it is reasonable to conclude that swirl vortex type is not a major factor with regard to the aerodynamic performance of axial-flow compressors of this type. If lower hub-to-shroud radius ratios are used, there may be some influence on performance associated with the different maximum

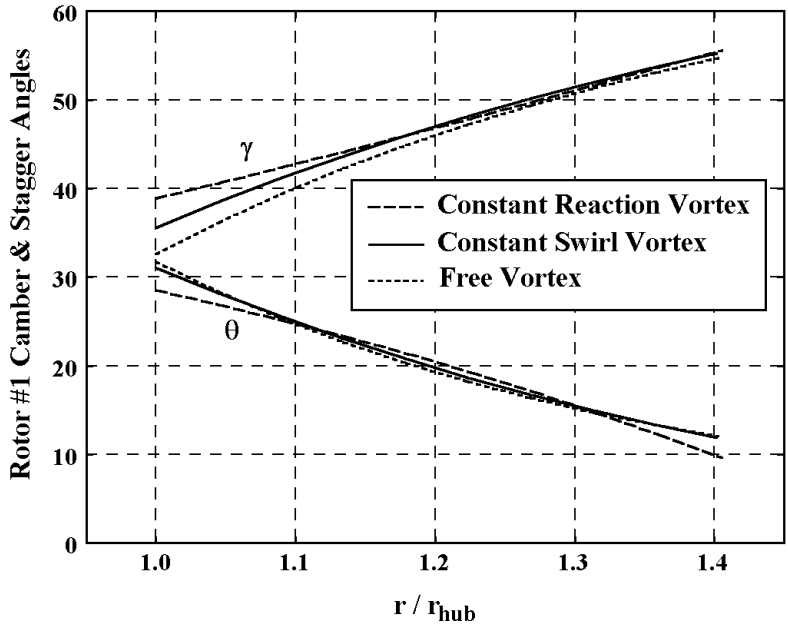

FIGURE 11-20 Comparison of Rotor Blade Geometry

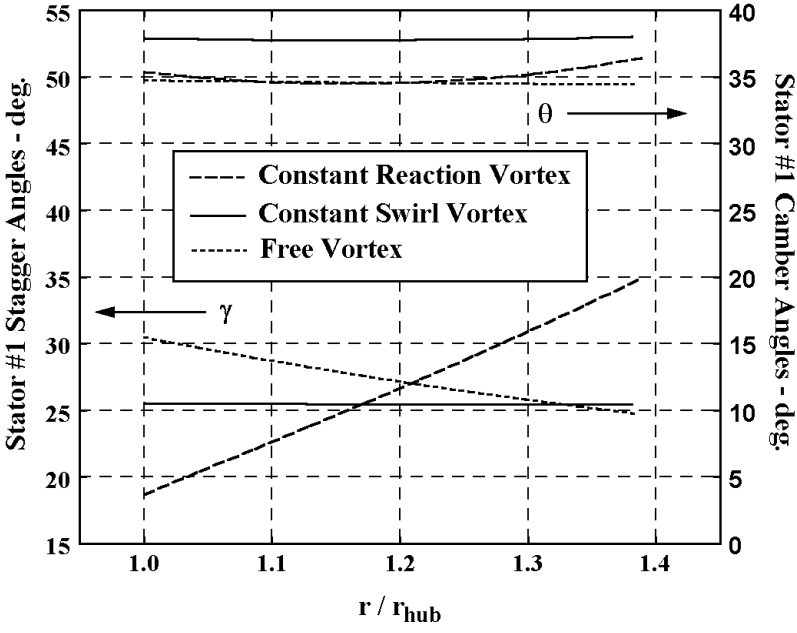

FIGURE 11-21 Comparison of Stator Blade Geometry

inlet relative Mach number levels or extremes in flow diffusion levels produced by the alternate swirl vortex types. But, in general, suitability to the design strategy and objectives, along with the cost and ease of manufacturing of the blades, are more likely to be the basis for selecting the swirl vortex type.

11.8 RISKS AND BENEFITS

The benefits from the present axial-flow compressor aerodynamic design procedure should be relatively clear from the examples presented in this chapter. The input specifications required are rather modest considering the complex design problem involved. The input specifications are relatively easy to supply, and provide the designer with substantial control over the aerodynamic features considered most critical to the design objectives. The tedious process of sizing the annulus, selecting blades and fitting them into the available space is left to the computer. The design process is guided by continual feedback from a performance analysis for the design mass flow rate and rotation speed. When a viable candidate design is identified, the design system can create an input file for the aerodynamic performance analysis to permit an evaluation of its off-design performance characteristics.

To obtain full benefit from the design system, on-demand monitor screen displays of tabular and graphical data are essential. End-wall contour geometry, blade geometry, relative and absolute flow data, blade row performance data and end-wall boundary layer analysis data are essential to evaluate the designs. Graphical display of the equivalent velocity ratios, W_{RE}, is particularly useful when attempting to tailor the flow diffusion distributions similar to the examples presented in this chapter. It has been noted that the capability to specify stage performance for a few key stages and to interpolate for intermediate stages can simplify the input specifications. The same is true for specifying the fixed end-wall contour data. Specifying axial spacing is often simpler than specifying axial coordinates. Provision to enter radii at some stations and to interpolate for intermediate stations is also a useful simplification. It is important to use a representative blade tip clearance, but it is usually sufficient to use a constant value for all blade rows. Monitor screen displays of the actual blade profiles at any radius are also useful, and the design system should have the capability to export blade profile coordinates for the drafting and manufacturing of the blades. Figure 11-22 is an example of these data obtained from the design of Compressor B.

It is important to recognize that the substantial benefits of this design system also introduce a level of risk that requires designers to exercise judgment. Chapters 6 through 9 present numerous procedures used in the process of predicting the performance of axial-flow compressors. All of those methods involve a significant level of approximation. A performance analysis is normally qualified against experimental data to fine-tune it until it offers sufficient prediction accuracy for the intended applications. In general, none of the cases considered in such a qualification study will be evaluated by the performance analysis as completely optimized. But the present design system provides the unique situation of producing an axial-flow compressor design that is precisely optimized to the models used in the performance analysis. Since those models are far from exact,

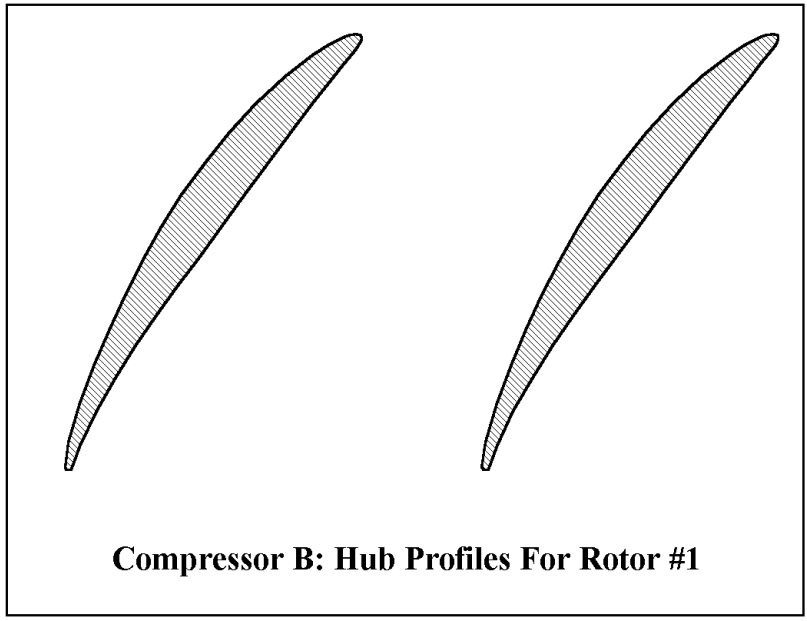

FIGURE 11-22 Typical Blade Profiles

the present design approach will inevitably expose the weaknesses in those models. The most obvious risk is that the predicted design point efficiency is likely to be overestimated. In the examples presented in this chapter, every blade row is operating precisely at its minimum loss condition on all stream surfaces. It is highly unlikely that the empirical models of Chapter 6, the through-flow analysis of Chapter 7 and the boundary layer analysis of chapter 8 are all sufficiently accurate to actually produce that situation throughout a multistage compressor. This design system should provide a very good design, but probably not as good as will be indicated by the performance analysis. Indeed, experienced turbomachinery aerodynamic designers are quite aware of the risk involved with designing directly with the performance analysis that will be used to evaluate the design. The axial-flow compressor is somewhat unique in that it is rather easy to convert a performance analysis to a design system of the type described in this chapter. The substantial benefits provided certainly justify taking advantage of this opportunity, but definitely require considerable judgement by the designer to maintain realistic expectations for the resulting design.